ACS NANO
Cite This: ACS Nano 2019, 13, 4111−4123
www.acsnano.org

ARTICLE

Interfacial Assembly of Tunable Anisotropic Nanoparticle Architectures

Tsung-Yeh Tang,[†,§] Yilong Zhou,[‡,§] and Gaurav Arya*[,‡]

[†]Department of NanoEngineering, University of California, San Diego, La Jolla, California 92093, United States
[‡]Department of Mechanical Engineering and Materials Science, Duke University, Durham, North Carolina 27708, United States

Supporting Information

ABSTRACT: We propose a strategy for assembling spherical nanoparticles (NPs) into anisotropic architectures in a polymer matrix. The approach takes advantage of the interfacial tension between two mutually immiscible polymers forming a bilayer and differences in the compatibility of the two polymer layers with polymer grafts on particles to trap NPs within two-dimensional planes parallel to the interface. The ability to precisely tune the location of the entrapment planes *via* the NP grafting density, and to trap multiple interacting particles within distinct planes, can then be used to assemble NPs into unconventional arrangements near the interface. We carry out molecular dynamics simulations of polymer-grafted NPs in a polymer bilayer to demonstrate the viability of the proposed approach in both trapping NPs at tunable distances from the interface and assembling them into a variety of unusual nanostructures. We illustrate the assembly of NP clusters, such as dimers with tunable tilt relative to the interface and trimers with tunable bending angle, as well as anisotropic macroscopic phases, including serpentine and branched structures, ridged hexagonal monolayers, and square-ordered bilayers. We also develop a theoretical model to predict the preferred positions and free energies of NPs trapped at or near the interface that could help guide the design of polymer-grafted NPs for achieving target NP architectures. Overall, this work suggests that interfacial assembly of NPs could be a promising approach for fabricating next-generation polymer nanocomposites with potential applications in plasmonics, electronics, optics, and catalysis where precise arrangement of polymer-embedded NPs is required for function.

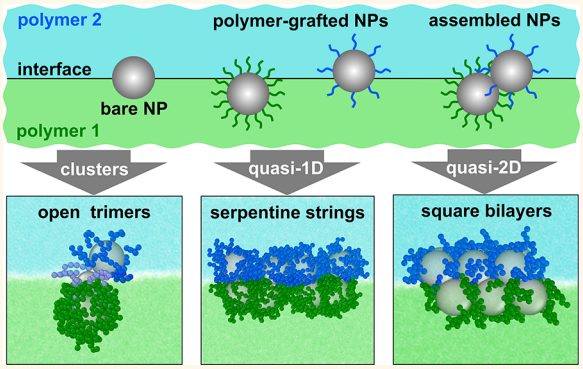

KEYWORDS: *nanoparticle assembly, polymer−polymer interface, anisotropic structures, molecular dynamics simulations, polymer nanocomposites, polymer-grafted nanoparticles*

Polymer-nanoparticle composites have attracted considerable scientific and technological interest in the past few decades. While many traditional applications of such composites require the nanoparticles (NPs) to remain well dispersed within the polymer matrix, some of the newer proposed applications rely on higher-order organization of NPs.[1] For instance, by arranging plasmonic NPs into nonclose-packed clusters and periodic arrays, one could take advantage of the distinct plasmonic couplings between particles to create optically active composites.[2−6] Similarly, the organization of magnetic, semiconducting, or mixtures of semiconducting and plasmonic NPs into specific arrangements results in distinct magnetic, exciton, or plasmon-exciton couplings that may be harnessed for novel applications.[1,7−11] Self-assembly provides a powerful bottom-up approach for organizing NPs in a highly parallelized fashion. However, achieving precise, complex, and exotic assemblies of NPs in polymers is challenging. Inorganic NPs are usually polydisperse in size and immiscible in polymers (due to strong interparticle van der Waals interactions, solvophobic surfaces, and polymer-mediated depletion forces), which cause the particles to kinetically agglomerate into random fractal structures.[12−14] Even if the NPs were homogeneous and their interactions were weakened to access thermodynamically favored structures, the spherical NPs typically used for assembly would result in close-packed "isotropic" structures that maximize the total number of favorable contacts between the particles.

Several strategies have been proposed to promote NP assembly into "anisotropic" structures that go beyond the isotropic morphologies obtained with spherical NPs. An obvious strategy is to use shaped particles,[15−18] which can now be routinely synthesized due to advances in inorganic synthesis methods. A related approach is to adsorb or graft

Received: November 15, 2018
Accepted: March 18, 2019
Published: March 18, 2019

DOI: 10.1021/acsnano.8b08733
ACS Nano 2019, 13, 4111−4123

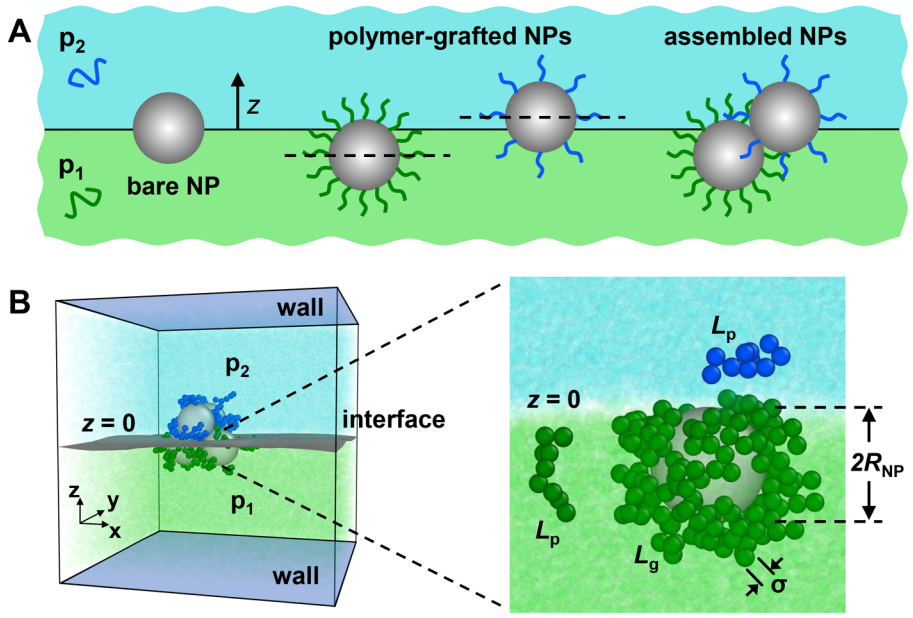

Figure 1. Interfacial assembly of NPs into anisotropic clusters and phases. (A) Schematic of the proposed strategy: Bare NPs neutral to both polymer layers p_1 and p_2 of a bilayer get trapped symmetrically at the interfacial plane. Grafting NPs with chains selective to p_1 displaces the NP downward to a new equilibrium position. Grafts selective to p_2 displace the NPs upward, but by a smaller distance if the chains are grafted at lower density. Mixtures of such NP species assemble into unusual configurations that minimize the overall free energy of the system. A tilted NP dimer assembled in this manner is shown for illustration. (B) Simulation setup and coarse-grained model of the polymer bilayer and polymer-grafted NPs used for demonstrating interface-mediated assembly of NPs. Throughout this study, the top and bottom polymer layers are shown in cyan and fluorescent green, the NP cores are colored gray, and the grafts selective to the two layers are shown in blue and green.

functional groups non-uniformly across the surface of the NPs, resulting in "patchy" particles that interact asymmetrically with each other.[19−21] Though these approaches have yielded encouraging assembly outcomes in aqueous media, achieving similar levels of success in polymeric media has been challenging. A third approach involves grafting polymer chains onto the surface of the NPs.[22] In addition to improving the polymer miscibility of the NPs, this strategy also introduces anisotropic interactions between NPs due to "polarization" of the distribution of grafted chain segments around NPs when they get close to each other.[23,24] In this manner, spherical NPs have been assembled into anisotropic structures like sheets and strings by simply varying the grafting density or the length of the grafted chains.[23] Researchers have also used microphase separation of block copolymers to trap small NPs within or at the interface of the formed domains,[25−29] providing an avenue for spatially organizing the NPs. Other approaches involving the use of magnetic and electric fields to align particles also hold promise for directing NP assembly toward anisotropic structures but have so far been applied mostly to micron-sized particles in aqueous systems.[30−32]

Here we propose a distinct strategy for assembling NPs into anisotropic structures within a polymer matrix, as depicted schematically in Figure 1A. Our approach is motivated by the well-known phenomenon of colloids migrating to gas−liquid or liquid−liquid interfaces to reduce their surface energy.[33−36] We take advantage of this effect to trap NPs at the interface between two mutually immiscible polymers forming a stable bilayer. Thus, NPs that interact similarly with both polymer layers would be expected to localize at the interfacial plane, where they can occlude the largest possible area of the interface and thereby provide the largest free energy benefit. Consider now multiple such NPs that also exhibit strong attractive interactions among themselves. While this scenario may facilitate the formation of free-floating planar sheets of NPs, it is not particularly useful for assembling more exotic structures. To address this shortcoming, we suggest trapping of NPs at *multiple, distinct* planes parallel to the interfacial plane, where the spacing between adjacent planes is small enough to allow the NPs to interact, and potentially assemble, across the planes. For instance, two NPs on opposite sides of the interfacial plane at normal displacements smaller than the particle radii should still be able to interact with each other to potentially form a tilted NP dimer. To achieve control over the normal positioning of NPs relative to the interfacial plane, we propose grafting the NPs with polymer chains that are preferentially miscible with one of the two polymer layers. Selective interactions of the grafts should then provide the necessary thermodynamic driving force to displace NPs away from the interfacial plane, and the extent of grafting, a controllable experimental parameter, should be able to provide precise control over the extent of this normal displacement of particles. In the following sections, we demonstrate using computer simulations the ability of the proposed assembly strategy to obtain NP architectures currently not achievable by conventional approaches.

RESULTS AND DISCUSSION

To demonstrate and further investigate the proposed assembly approach, we carried out molecular dynamics (MD) simulations of polymer-grafted NPs in a polymer bilayer formed by two mutually immiscible polymers. Since our primary aim is to elucidate general features of the assembly mechanism and *not* to model any specific system, we used a coarse-grained (CG) model to represent the polymer chains and NPs, which also kept computational costs reasonable

DOI: 10.1021/acsnano.8b08733
ACS Nano 2019, 13, 4111−4123

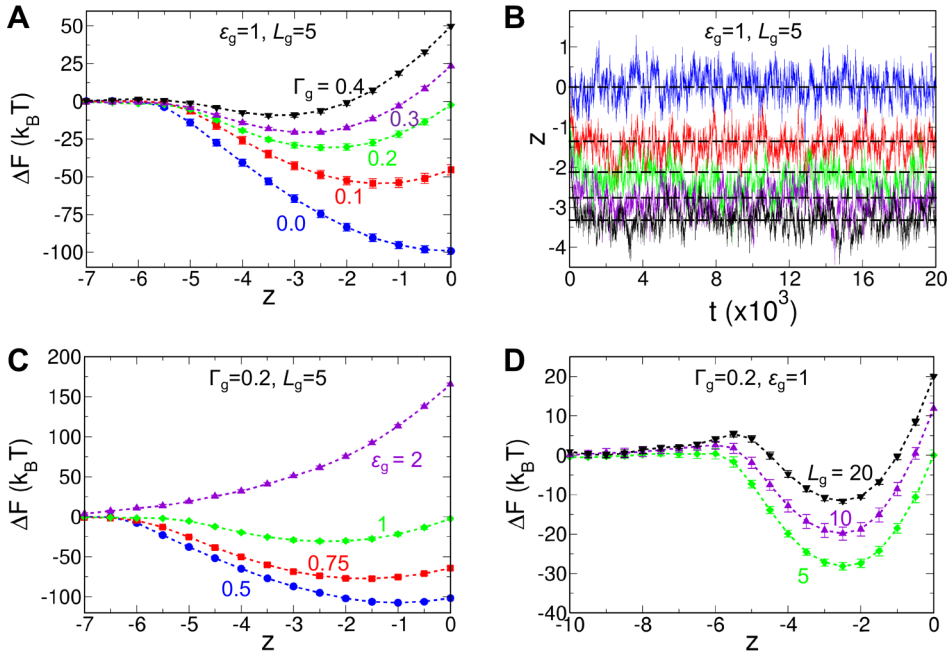

Figure 2. Free energy profiles of polymer-grafted NPs as a function of their position from the interfacial plane. (A) $\Delta F(z)$ for NPs with grafting densities Γ_g = 0.1, 0.2, 0.3, and 0.4 chains/σ^2 compared against that of a bare NP (Γ_g = 0). (B) Fluctuations in position $z(t)$ of NPs as a function of time t captured from MD simulations of free particles in the bilayer. The five trajectories correspond to the five species of NPs examined in (A). Dashed lines correspond to the equilibrium positions z_m obtained from the $\Delta F(z)$ profiles. (C) $\Delta F(z)$ for NPs grafted with chains that are equally incompatible to polymer p_2, but exhibit different compatibility with polymer p_1 (ε_g = 0.5, 0.75, 1, and 2ε). (D) $\Delta F(z)$ for NPs grafted with chains of different lengths L_g = 5, 10, and 20 beads.

(Figure 1B, left). Briefly, the NP grafts and the matrix chains of the bilayer (denoted by "g", and "p_1" and "p_2") were treated as bead-chains[37] in which polymer segments are represented by beads, and the NP cores (denoted by "NP") were treated as rigid spheres. Chains of the same polymer type were considered to be miscible, and hence their segments interacted with each other *via* a potential that accounts for attractive and excluded-volume interactions. In contrast, the two polymer layers were considered immiscible, and hence their inter-segmental interactions were treated using a potential that accounts only for excluded-volume interactions. The grafts were considered to be either partly or fully miscible with one layer and immiscible with the other, and their interactions were again treated using the above two kinds of potentials. Attractive and excluded-volume potentials were also used for modeling interactions between NP cores and between NP cores and polymer segments. The size σ of polymer beads and the strength ε of attraction between like segments set the length and energy scale of the system. This simple model captures the essential physics of the NP-bilayer system, including the conformational dynamics of the polymer chains, interactions between tethered and free chains, depletion forces exerted by the matrix, and diffusion of grafted particles in polymers.[24,38] Furthermore, the potentials used for treating miscible and immiscible interactions have been shown to yield stable bilayers that reproduce the density profiles, surface tension, and capillary fluctuations of fluid interfaces.[39−41]

The MD simulations were performed in the canonical ensemble at a fixed temperature of $T = \varepsilon/k_B$ and a fixed density of 0.85 beads/σ^3, wherein the system is present in a melt-like state. Periodic boundary conditions were implemented in the x and y directions parallel to the interface and rigid walls were used in the normal direction z (Figure 1B, right). A sufficiently large simulation box was chosen in the normal and lateral directions to prevent artifacts from the confining wall and periodic boundaries, respectively. The chain lengths of both matrix polymers were fixed at L_p = 10 beads. The radii of the NP cores were set to $R_{NP} = 3\sigma$, unless otherwise stated, and their surfaces were isotropically grafted with chains; Graft lengths of L_g = 5−20 beads and grafting densities of Γ_g = 0−0.4 chains/σ^2 spanning the mushroom to weak-brush grafting regimes were explored. The strength of attraction ε_g between graft segments and those of the layer miscible to them were varied in the range 0.5−2ε, and an attraction of $\varepsilon_{NP} = 50\varepsilon$ was used for modeling inter-NP interactions.

Particle Trapping at Interface. We first examined the behavior of *individual* NPs in polymer bilayers to determine how NP grafting with chains selective to one of the polymer layers affects the interfacial location of the particles. While MD simulations can directly provide the 3D trajectory of a NP as a function of time t from which one could obtain its ensemble-averaged *normal* position $\langle z(t) \rangle$ relative to the interfacial plane (represented by $z = 0$), we used an alternative, more informative route to determining the preferred positions of the NPs. Specifically, we used simulations to compute the free energy (potential of mean force) $\Delta F(z)$ of the NP-polymer system as a function of particle displacement z from the interfacial plane; the delta symbol is meant to emphasize that this free energy is obtained *relative* to the free energy of the reference system in which the NP is located far from the interface, in the bulk of the polymer layer miscible with the NP grafts. The location of the global minimum in $\Delta F(z)$, denoted

DOI: 10.1021/acsnano.8b08733
ACS Nano 2019, 13, 4111−4123

by z_m, should then provide us the most energetically favorable (equilibrium) position of the NP. In addition to equilibrium positions, this free-energy-computation route reveals the energetic basis of particle trapping not possible to obtain from NP trajectories alone and also enables quantitative comparison with the theoretical model of NP trapping developed further below.

To study the effect of grafting, we computed $\Delta F(z)$ for NPs of radii $R_{NP} = 3\sigma$ grafted with chains of length $L_g = 5$ beads that are miscible with one polymer layer (p_1) and immiscible with the other (p_2). For convenience, we chose the grafts to be chemically identical to p_1 chains (*i.e.*, $\varepsilon_g = \varepsilon$). We examined NPs with four different grafting densities Γ_g in the range 0.1 to 0.4 chains/σ^2. For comparison, we also computed $\Delta F(z)$ for a bare NP. Figure 2A presents these computed free energy profiles, all of which exhibit a parabolic dependence on z and contain a single minimum. These minima, representing equilibrium positions z_m of particles, shift away from the interfacial plane and toward the layer compatible with the grafts, with increasing grafting density. Compared to the bare NP that prefers to reside at the interfacial plane ($z_m = 0$), the NP with the largest grafting density Γ_g considered here gets displaced by a distance ($z_m \approx -3.25\sigma$) almost as large as the NP radius. The equilibrium positions z_m obtained from the free energy profiles agree well with the average positions $\langle z(t)\rangle$ obtained from simulations of freely mobile NPs (Figure 2B). Note that even though z_m reports the most favorable position while $\langle z(t)\rangle$ reports the ensemble-averaged position, the two quantities are expected to be similar for systems exhibiting a deep and symmetric energy well at the minimum, as observed for our NPs.

The bare NP's preference for the interfacial plane is obviously due to the particle occluding the largest possible area of the interface at this position, which leads to the largest reduction in the interfacial free energy. The free energy gain of $\Delta F(z_m) \sim -100 k_B T$ indicates very strong trapping of the NPs; larger particles, in the colloidal range, have been reported to exhibit even stronger trapping.[33,42,43] For the grafted NPs, even though their displacement away from the interface reduces the interfacial area occluded by the particle, the resulting increase in the interfacial free energy is more than compensated by favorable interactions between NP grafts and surrounding matrix that are gained as a result of the displacement. This gain arises from both the increase in favorable interactions of the grafts with the polymer layer compatible with them and the decrease in unfavorable interactions of the grafts with the incompatible layer. The higher the grafting density, the higher the gain in favorable graft-matrix interactions, and the more the particle displaces from the interfacial plane. At sufficiently high grafting density ($\Gamma_g \gtrsim 0.4$), the free energy gain arising from these favorable graft-matrix interactions overwhelms the gain in free energy arising from interface occlusion, causing the NPs to completely detach from the interface and move into the bulk of the polymer layer compatible with the grafts.

We also studied the effects of two additional parameters related to the grafts: the extent of their miscibility with the compatible polymer layer as quantified by the interaction strength ε_g, and their length L_g. Figure 2C shows the $\Delta F(z)$ profiles computed for grafted NPs with ε_g in the range 0.5 to 2ε, keeping other grafting parameters fixed ($L_g = 5$ beads and $\Gamma_g = 0.2$ chains/σ^2). The free energy profiles retain the characteristic parabolic shape obtained earlier, and the equilibrium position shifts away from the interface with increasing magnitude of ε_g until the NPs completely detach from the interface and go into the bulk phase at $\varepsilon_g \gtrsim 1.5$. Figure 2D shows the free energy profiles obtained for varying graft lengths between $L_g = 5$ and 20 beads with fixed $\Gamma_g = 0.2$ chains/σ^2 and $\varepsilon_g = \varepsilon$. In contrast to the trends obtained with varying Γ_g or ε_g, the equilibrium positions surprisingly show little to no change with increasing magnitude of L_g. A likely source for this insensitivity is the flexibility of the grafts that allows the longer grafts facing the incompatible polymer layer to bend "backwards" to avoid unfavorable interactions with this layer and maximize favorable interactions with the compatible layer (Figure S1). This effect apparently allows the NPs to maintain the same amount of favorable graft-matrix interactions (interactions with miscible layer minus those with immiscible layer) regardless of the graft length. Interestingly, NPs with long grafts (especially those with $L_g = 20$ beads) lead to a shallow energy barrier as the particle approaches the interface from the side of the compatible polymer layer ($-6.5\sigma < z < -4.5\sigma$) that also likely arises from this backward bending of grafts, which leads to some loss of their conformational entropy.

The above results demonstrate that NPs grafted with chains selective to one of the layers of a polymer bilayer provides a viable approach for trapping NPs at normal positions located roughly within a radius of the particle on either side of the interface ($|z_m| \lesssim R_{NP}$). We also illustrated that the equilibrium displacement z_m of the NPs from the interface can be effectively tuned by modulating the surface density of the grafts or the difference in their compatibility with the two polymer layers, though the former perhaps offers the best control and range from an experimental standpoint. Hence, in the remainder of this work, we use the grafting density as our "knob" (keeping the length and miscibility of the grafts fixed at $L_g = 5$ and $\varepsilon_g = \varepsilon$) to tune the positions, and thereby the interactions between polymer-grafted NPs at polymer–polymer interfaces.

Theoretical Model of Trapping. The free energy profiles and equilibrium positions computed from simulations can be described by a simple model, enabling quantitative prediction and explanation of the observed effects of NP grafting. To obtain this model, we considered the migration of a NP from the bulk region of the polymer layer compatible with its grafts (say p_1) to a distance z from the interfacial plane where the NP intersects it (Figure 3A). The free energy change associated with this migration is made up of two contributions: $\Delta F(z) = \Delta F_{int}(z) + \Delta F_{graft}(z)$. The first term given by $\Delta F_{int} \equiv -\gamma_{p_1-p_2} A_{p_1-p_2}(z) < 0$ represents the gain in free energy due to the NP occluding part of the interface, where $\gamma_{p_1-p_2}$ is its surface tension and $A_{p_1-p_2}$ is its circular area occluded by the NP. The second term $\Delta F_{graft} \equiv \Delta\gamma'_{g-p} A_{g-p_2}(z) > 0$ represents the loss in free energy caused by the replacement of part of the favorable interactions of the grafts with the compatible chains of layer p_1 for unfavorable interactions with incompatible chains of layer p_2 across the interface, where $\Delta\gamma'_{g-p}$ is the difference in the surface energies of the grafts interacting with

DOI: 10.1021/acsnano.8b08733
ACS Nano 2019, 13, 4111–4123

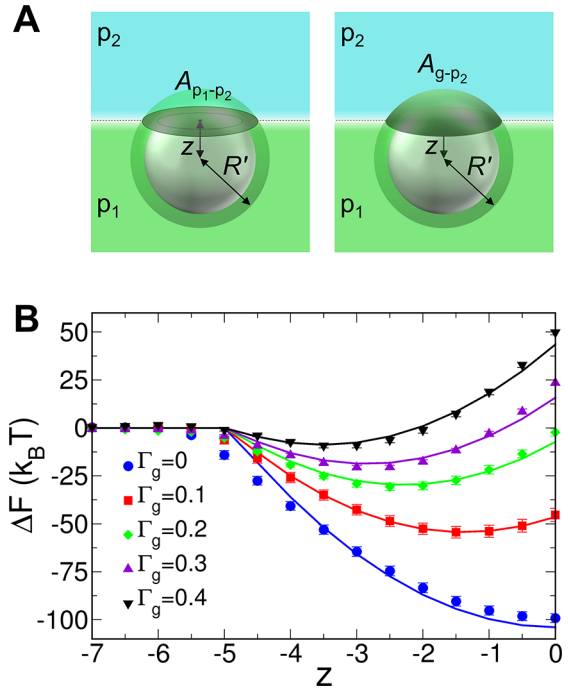

Figure 3. Free energy model for NP trapping at interfaces. (A) Schematic showing the two main contributions to the free energy in this model: loss in interfacial surface energy proportional to the circular cross-sectional area $A_{p_1-p_2}$ occluded by the polymer-grafted NP, and gain in the surface energy of the grafts with the surrounding polymer matrix proportional to the area A_{g-p_2} of the spherical cap contacting the incompatible polymer p_2. (B) Model fits (solid lines) to the free energy profiles computed from simulations (symbols) for bare NPs and NPs grafted with chains at the four grafting densities shown in Figure 2A.

the two layers and A_{g-p_2} is the area of the spherical cap of grafts in contact with layer p_2. The prime symbol is used for differentiating such energies from the surface tension traditionally applied to interfaces formed between *free* polymer chains. By writing down the two area terms in terms of effective radii $R' > R_{NP}$ of NPs that includes the graft contribution, we arrive at the following expression for the free energy change we seek (see Supporting Information and the associated Figures S2 and S3 for complete derivation):

$$\Delta F(z) = \begin{cases} 0 & z \le -R' \\ -\pi(R'^2 - z^2)\gamma_{p_1-p_2} + 2\pi R'(R' + z)\Delta\gamma'_{g-p} & |z| < R' \\ 4\pi R'^2 \Delta\gamma'_{g-p} & z \ge R' \end{cases} \quad (1)$$

The above expression yields a quadratic dependence of ΔF in position z, explaining the parabolic shapes of the computed free energy profiles in Figure 2A. The equilibrium position of the NPs may be obtained *via* $\partial\Delta F/\partial z|_{z_m} = 0$, yielding $z_m = -(\Delta\gamma'_{g-p}/\gamma_{p_1-p_2})R'$. This result suggests that the NPs prefer to stay at the interfacial plane when they are equally selective to both polymer layers ($\Delta\gamma'_{g-p} = 0$), and get increasingly displaced from this position with increasing difference in the compatibility of the NP with the two layers (increasing $\Delta\gamma'_{g-p}$), predictions consistent with our simulations. The model also predicts that no minimum exists for $\Delta\gamma'_{g-p} > \gamma_{p_1-p_2}$ when the NPs become too selective for one of the layers and prefer to remain fully immersed in it. The relative stability of the NP to reside at locations intersecting the interfacial plane, as compared to the bulk, is given by $\Delta F(z_m) = -\pi R'^2(\gamma_{p_1-p_2} - \Delta\gamma'_{g-p})^2/\gamma_{p_1-p_2}$. Thus, the NPs that exhibit the highest interfacial stability are those that are neutral to both polymer layers $\Delta\gamma'_{g-p} = 0$ and thereby position themselves at the interfacial plane to occlude the largest possible area of the interface without sacrificing any favorable graft-matrix interactions. The stability decreases as the NP-matrix interactions become more asymmetric ($\Delta\gamma'_{g-p} \neq 0$), and the NPs get increasingly displaced away from the interfacial plane. Another consequence of the quadratic nature of this model is its curvature $\kappa \equiv \partial^2\Delta F/\partial z^2 = 2\pi\gamma_{p_1-p_2}$ that, interestingly, depends *only* on properties of the bilayer (its interfacial tension) and *not* of the grafted NPs (*e.g.*, their size or interactions). This result also implies that the NPs trapped at the interface should exhibit similar fluctuations δz in their normal position irrespective of NP size or interactions, given that $\delta z \sim \sqrt{k_B T/\kappa}$. Indeed, the computed free-energy profiles for the various NPs explored here appear to display similar curvatures (Figure 2A,C,D), and the trapped NPs appear to exhibit similar extents of fluctuations irrespective of their grafting density (Figure 2B). Our model is thus able to *qualitatively* explain all observed trends in the computed free energy profiles.

We also investigated the ability of our model to *quantitatively* fit the free energy profiles computed from simulations by setting $R' = 4.95\sigma$ and using the unknown $\gamma_{p_1-p_2}$ and $\Delta\gamma'_{g-p}$ as adjustable parameters. Since the bilayer was kept the same across all systems, $\gamma_{p_1-p_2}$ in the model was kept unchanged across all profiles during the fitting procedure. However, $\Delta\gamma'_{g-p}$, which is expected to vary with the grafting density, was adjusted independently for each profile. Figure 3B shows model fits obtained for the bare NP and the grafted NPs at the four grafting densities simulated here. We find that the model does an excellent job in fitting all profiles. There are slight discrepancies at $z < -R'$ where our model enforces ΔF to instantly flatten out as the NPs no longer contact the interface, whereas the computed profiles indicate a more longer-ranged effect of the interface, albeit weak, that extends to distances as large as $\sim 6\sigma$. This effect could arise from multiple factors not accounted in this model, including capillary fluctuations of the interface and stretching of NP grafts or the deformation of the interface to remain in mutual contact, as depicted in Figure S4. The model also does an excellent job in predicting the equilibrium positions of the NPs for both the bare and grafted NPs (Figure S5a). In addition, the fitted value of $\gamma_{p_1-p_2}$ compares favorably to surface tensions estimated from theory and those measured experimentally, and the fitted values of $\Delta\gamma'_{g-p}$ also seem physically reasonable (see Supporting Information and Figure S5b).

Assembly of Interfacial Clusters. Having demonstrated how a polymer bilayer could be used to trap polymer-grafted NPs in 2D planes parallel to the interface and how the NP grafting density could be used to control the position of these NP traps, we next investigated how the interactions between *multiple* such NPs trapped within different planes could be harnessed to assemble NPs into unconventional configurations. We began by probing the assembly of *two* "anti-symmetric"

DOI: 10.1021/acsnano.8b08733
ACS Nano 2019, 13, 4111−4123

polymer-grafted NPs identical in all aspects *except* that they are grafted with chains compatible with opposite layers of the bilayer. Based on our earlier results, we anticipated that the two NPs would partition into opposite sides of the interfacial plane while still intersecting partly with it, thereby allowing for interactions between the NPs across the interface. To examine how these interactions manifest into assembly, we simulated the dynamics of two such NPs within a bilayer, starting from a well separated configuration of NPs, where they were present in their respective layers at distances $z = \pm R_{NP}$ sufficiently far from the interface but well within the influence of the interfacial trap. As earlier, we studied NPs of size $R_{NP} = 3\sigma$ grafted with chains of length $L_g = 5$ beads at four different grafting densities in the range $\Gamma_g = 0.1$ to 0.4 chains/σ^2 with bare NPs as control. In each simulation, one NP had grafts chemically identical to the chains of layer p_1 with attraction strength $\varepsilon_g = \varepsilon$, and the other to p_2, also with $\varepsilon_g = \varepsilon$.

Our simulations show that the *bare* NPs assembled into a stable dimer whose axis is oriented horizontally, parallel to the interface (Figure 4A). The assembly was found to occur *via*

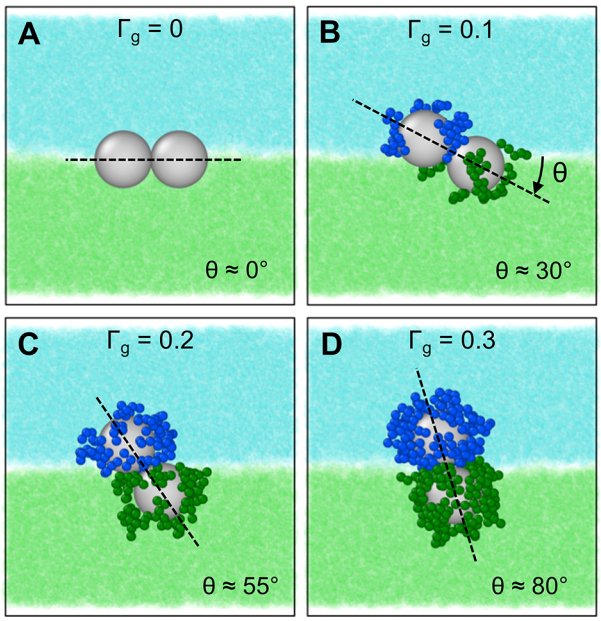

Figure 4. NP dimers with a tunable tilt relative to the interface assembled from antisymmetric polymer-grafted NPs. Representative configurations taken from simulations illustrate how dimers become increasingly tilted with increasing grafting density, exhibiting average tilt angles of (A) $\theta \approx 0°$ for bare NPs, (B) $\theta \approx 30°$ for $\Gamma_g = 0.1$ chains/σ^2, (C) $\theta \approx 55°$ for $\Gamma_g = 0.2$ chains/σ^2, and (D) $\theta \approx 80°$ for $\Gamma_g = 0.3$ chains/σ^2. Dimer axes are shown as dashed lines.

two pathways: The two NPs diffused and migrated to their preferred location, the interfacial plane, before colliding with each other to form a horizonally aligned dimer; or the NPs collided and stuck to each other before reaching the interface to yield a tilted dimer, which eventually rotated into the preferred horizontal orientation. The *grafted* NPs of low to medium grafting densities (Γ_g = 0.1–0.3 chains/σ^2) also exhibited similar assembly dynamics, *except* that they partitioned to their off-centered locations above and below the interface, and yielded stable NP dimers whose center of masses remain at interfacial plane ($z_{com} \approx 0$) but whose axes display a visible tilt relative to the interface (Figure 4B–D). Interestingly, the tilt angle increases with increasing grafting density. This effect results from the NP cores attempting to maintain contact with each other (as a result of strong but short-range attraction between them) without sacrificing the free energy gained from the interface. Due to this geometric constraint, the tilt angle θ can be easily predicted as $\theta = \sin^{-1}(|z_m|/R_{NP})$, where $|z_m|$ is the equilibrium distance of either NP from the interfacial plane in isolation. Comparison of the predicted tilt angles with those measured directly from simulations reveals good agreement between the two sets of angles (Figure S6), confirming that NPs indeed prefer to stay within their interfacial traps z_m, largely unhindered by the presence of the other particle. At sufficiently high grafting densities ($\Gamma_g = 0.4$ chains/σ^2), the NPs stay relatively far from the interface, and even when the two NPs collide with each other, they are unable to form a stable dimer, arguably due to strong steric repulsion between their grafts. Thus, interfacial trapping of NPs could indeed be used to assemble *antisymmetric* dimers of NPs, and moreover tune their orientation with respect to the interface. It should be straightforward to extend these results to *asymmetric* dimers, where the two NPs have different sizes or grafting densities. In both cases, the particles will prefer to reside at different absolute distances $|z_{m,1}| \neq |z_{m,2}|$ from the interface, resulting in dimers that are overall shifted from the interfacial plane ($z_{com} \neq 0$) and exhibit a tilt angle $\theta = \sin^{-1}[(|z_{m,1}| + |z_{m,2}|)/(R_{NP,1} + R_{NP,2})]$, where $R_{NP,1}$ and $R_{NP,2}$ are the core radii of the two NPs.

The NP-trapping approach could also be used to assemble *larger* anisotropic clusters encompassing more than two species of NPs. As demonstration, we attempted to assemble *open* NP trimers with a tunable "bending" angle, defined as the angle φ subtended by the two terminal NPs about the middle NP. Clearly, such configurations cannot be achieved using bare NPs, which would simply assemble into *closed* triangles, both in the bulk phase and at an interface. To this end, we proposed grafting the three NPs with distinct types and/or numbers of chains to trap them at different distances from the interfacial plane in such a way that the two terminal NPs cannot contact and stick to each other (Figure 5A). Specifically, we trapped the middle NP (labeled "NP2" in the figure) at the interface by leaving the particle bare or grafting it with chains neutral to both polymer layers. The other two NPs (labeled "NP1" and "NP3") were trapped on either sides of the interface by grafting them with chains selective to opposite polymer layers. To achieve the widest possible range of φ, one of these terminal NPs (NP1, say) was densely grafted to push it as far as possible into the bulk polymer phase without completely detaching from the interface, and the middle NP was kept sufficiently small so that it contacted NP1 in a perpendicular orientation. The other terminal NP (NP3) whose relative orientation with respect to NP2 could be modulated *via* its grafting density should then provide us a "knob" for tuning φ.

To test this strategy, we performed simulations of appropriately chosen polymer-grafted NPs in the bilayer. We used $R_{NP} = 3\sigma$ particles for the terminal NPs and graft lengths of $L_g = 5$ beads on all three NPs, as in the dimer simulations. As proposed, NP1 was densely grafted with chains miscible to p_1. We found that $\Gamma_g = 0.52$ chains/σ^2 pushed NP1 to $z \simeq 5\sigma$,

DOI: 10.1021/acsnano.8b08733
ACS Nano 2019, 13, 4111–4123

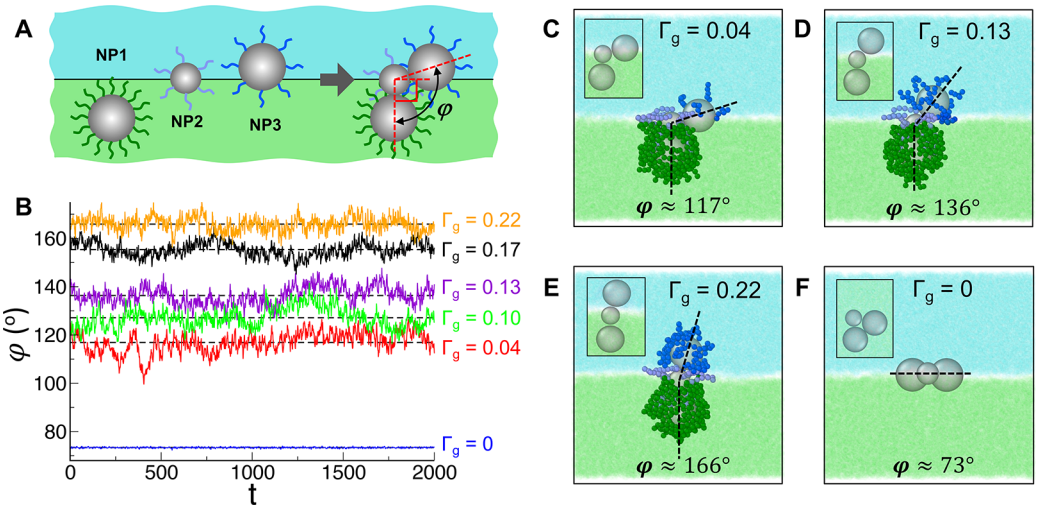

Figure 5. NP trimers with open and tunable bending angle assembled at the polymer interface. (A) Schematic of the strategy used for assembling such trimers involving three NPs (NP1, NP2, and NP3) grafted with different kinds of chains (see text for more details). (B) Bending angles $\varphi(t)$ obtained as a function of time t from simulations of trimer systems differing in the grafting density on NP3 (as specified), but fixed grafting densities on NP1 and NP2, respectively. (C–E) Representative configurations of these trimers captured from simulations with $\varphi \approx 117°$ (C), $\varphi \approx 136°$ (D), and $\varphi \approx 166°$ (E) obtained using grafting densities of 0.04, 0.13, and 0.22 chains/σ^2 on NP3 (insets show NP configurations more clearly without their grafts). (F) Representative configuration of a closed trimer with $\varphi \approx 73°$ obtained from bare NPs (inset shows top view for better visualization).

a position where its grafts barely touch the interface. NP2 was chosen to have a smaller size of $R_{NP} = 2$ so that it could bind to NP1 in a vertical orientation without sacrificing its equilibrium position ($z_m \approx 0$). While a bare particle could also yield this desired position and contact orientation, we chose to graft NP2 with neutral chains at a moderate grafting density of 0.32 chains/σ^2 given that grafting offers the additional benefit of stability against potential aggregation of NPs. While this is not an issue when studying isolated clusters, nonspecific aggregation of NPs could become problematic when examining the assembly of larger numbers of clusters at high concentrations. Lastly, NP3 was grafted with chains miscible to p_2, and its grafting density was varied between 0.04 and 0.3 chains/σ^2 to modulate the trapped position of NP3, and thereby modulate φ. As before, we used $\varepsilon_g = \varepsilon$ to treat all miscible interactions of NP1 grafts with p_1, NP2 grafts with p_1 and p_2, and NP3 grafts with p_2. All simulations were initiated from a dispersed configuration of NPs.

Figure 5B shows the results of these simulations in terms of the bending angle $\varphi(t)$ measured as a function of simulation time t for each successfully formed trimer post-assembly. Representative snapshots of several of these trimer configurations as captured from the simulations are provided in Figure 5C–E. Our results confirm the assembly of open trimers with the "bond" between NP1 and NP2 oriented vertically with respect to the interface, consistent with our design strategy. Equally important, the results confirm that the grafting density on NP3 could indeed be used to modulate the bending angle of the trimers. In particular, the lowest grafting density examined here yielded bending angles close to 115°, and increasing the grafting density gradually pushed NP3 away from the interface, yielding larger trimer angles. In this manner, we were able to achieve trimer bending angles between 115° and 180°. Also evident from Figure 5B is the absence of bending angle data for systems in which NP3 was grafted with $\Gamma_g > 0.22$ chains/σ^2. Though these systems were able to yield stable dimers of NP1 and NP2, the densely grafted NP3 was unable to bind sufficiently strongly to NP2 due to the combined effect of NP3 residing too far from the interface as a result of the strong grafting and NP2 being pulled away from the interface due to NP1. Finally, to confirm that bare NPs, even at interfaces, are unable to yield such open trimer configurations, we simulated the above NPs without any grafts. As anticipated, the three bare NPs migrated to the interface and assembled into a horizontally aligned trimer with a closed angle of approximately 73° (Figure 5F). Note that the smaller size of the middle NP compared to the end NPs makes $\varphi > 60°$.

Assembly of Interfacial Phases. Consider the small clusters of interfacial NPs assembled above. While clusters of densely grafted NPs are likely stable against further association with other NPs and clusters due to steric repulsion from their grafts, clusters of weakly grafted or bare NPs might continue to assemble if additional NPs were available. We sought to investigate the kind of macroscopic structures (phases) such NPs formed. A *single* species of NPs would be expected to assemble into a hexagonally packed monolayer (assuming sufficiently high surface tension and negligible or weak multibody interactions between bare or weakly grafted NPs[23,24]), and depending on the preferred positions z_m of its NPs, the monolayer will form at the interfacial plane or offset from it. However, the assembly outcome is less straightforward for *multiple* NP species, where the different NP species prefer to reside in distinct planes parallel to the interfacial plane. Here, the NPs would be expected to compete for their favorite locations at or displaced from the interfacial plane, while the system as a whole attempts to also maximize the net number of favorable contacts between the NPs.

To illustrate how this interplay between interfacial and interparticle forces leads to atypical assembly structures, we considered a binary system composed of equal numbers of the two antisymmetric NP species studied earlier in the context of tilted dimers. The two NP types prefer to occupy positions within 2D planes on opposites sides of the interface with an

DOI: 10.1021/acsnano.8b08733
ACS Nano 2019, 13, 4111–4123

interplanar distance $\Delta d = 2|z_m|$ that can be tuned *via* the grafting density from a value of 0 to a value as large as $2R'$, the effective diameter of the NPs. The two layers of NPs are therefore expected to interact with each other, especially for weakly grafted NPs where Δd is small, raising the possibility of forming interdigitated bilayered structures. In this work, we simulated the assembly behavior of $N = 12$ such NPs (6 particles of each species) with Γ_g in the range 0.05 to 0.3 chains/σ^2. The grafting densities were kept small enough to promote interactions between NPs across the interface and to also allow NPs to stick to each other, and the particle numbers were kept large enough to enable extrapolation of the resulting finite-sized structures to macroscopic phases. For comparison, we also simulated the assembly of 12 bare NPs in a bulk polymer and in a polymer bilayer.

Simulations of bare NPs showed that in the bulk they assembled into the expected close-packed structure resembling a truncated triangular dipyramid[44,45] (Figure 6A), while in the bilayer the NPs formed the expected interface-trapped hexagonally arranged monolayer[46] (Figure 6B). In the $N \to \infty$ limit, the bulk structure should morph into a hexagonal- or cubic-close-packed lattice, and the interfacial structure should continue growing into an infinite planar sheet with hexagonally arranged particles. In both these structures, as well as all ensuing structures, the interparticle spacings are consistent with the minimum of the NP-NP interaction potential given by $2R_{NP} + (2^{1/6} - 1)\sigma \approx 6.12\sigma$, which we denote by R^*.

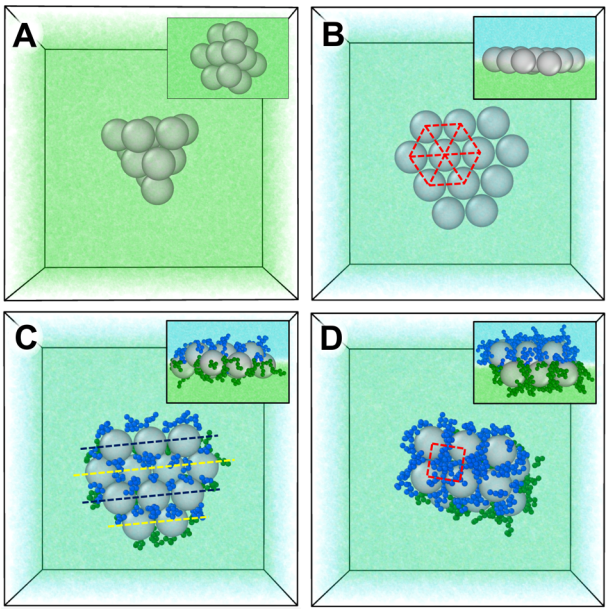

Figure 6. Higher-order structures of polymer-grafted NPs assembled at the interface of a polymer bilayer compared against those assembled using bare NPs. (A) Truncated triangular dipyramid obtained from bare NPs in a bulk polymer. (B) Hexagonal monolayer obtained from bare NPs in a bilayer interface. Red dashed lines show the underlying hexagonal packing. (C) Hexagonally ordered ridged monolayer obtained from grafted NPs ($\Gamma_g = 0.05$ chains/σ^2) in a bilayer. Black and yellow dashed lines indicate NPs located above and below the interface. (D) Squared-ordered bilayer obtained with grafted NPs ($\Gamma_g = 0.1$ chains/σ^2) in a bilayer. Red dashed lines emphasize square packing. Insets show structures from a view parallel to the interface.

Compared to these known structures, the symmetric grafted NPs assembled into unconventional structures in the bilayer. The NPs with the smallest grafting density of 0.05 chains/σ^2 assembled into a hexagonally arranged ridged monolayer comprised of alternating lines of NPs positioned $\approx 1.2\sigma$ above and below the interface (Figure 6C). These undulations obviously arise from the two species of NPs attempting to retain their preferred positions of $z_m \approx \pm 0.9\sigma$ on either side of the interfacial plane, as predicted for isolated NPs from eqs 2 and 6. As these NPs prefer to remain close to the interface, the NPs would have to sacrifice a larger amount of interfacial free energy to stretch apart to form a bilayer than the energy they would gain from the additional NP contacts provided by such a bilayer. Consequently, the NPs prefer to form a monolayer, albeit an undulating one, that exhibits a smaller number of favorable contacts, but occludes a large area of the unfavorable interface.

The NPs with slightly denser grafts ($\Gamma_g = 0.1$ chains/σ^2) form an interdigitated bilayer displaying a square arrangement of NPs in each layer (Figure 6D). Due to their stronger grafting, these NPs would individually prefer to reside farther from the interfacial plane ($z_m \approx \pm 1.4\sigma$ from eq 1). In the bilayer, these NPs are located roughly $\pm 2.16\sigma$ from the interfacial plane, indicating that the NPs get displaced by a small distance ($2.16\sigma - 1.4\sigma = 0.76\sigma$) from their preferred positions. Hence, the formation of a bilayer from such NPs leads to only a small sacrifice in the interfacial free energy, which is easily compensated by the interparticle interaction energy gained by the formation of the bilayer (8 contacts per NP in the bilayer *versus* 6 in the monolayer). A similar reasoning can be used to explain why the NPs prefer to form a square bilayer as opposed to a hexagonal bilayer that one might naively expect. Based on geometrical arguments (see Figure S7), the two NP layers of a close-packed hexagonal bilayer would be located at a distance $\pm R^*/\sqrt{6} \approx \pm 2.5\sigma$ from the interface and each NP would exhibit 9 contacts (6 within the layer and 3 in the other layer). Thus, the formation of a hexagonal bilayer, as opposed to a square one, would require larger displacements ($2.5\sigma - 1.4\sigma = 1.1\sigma$ *vs* 0.76σ) of the NPs from their preferred positions, while gaining only a single additional contact (9 *vs* 8 contacts). To rule out the distinct possibility that the square arrangement arose from any intrinsic tendency of NPs in each layer to form a square pattern (*e.g.*, due to multibody effects arising from the grafts), we performed simulations of the same system, but containing only one of the NP species. Our results show that each NP species, *on its own*, prefers to form a hexagonal monolayer (Figure S8), confirming that it is indeed interlayer interactions that are responsible for the formation of the square bilayer, which sacrifices much less interfacial free energy than a bilayer that had retained the hexagonal arrangement of the monolayers. Interestingly, simulations of systems with fewer NPs of one of the two species also reveal partial to perfect square arrangement of the NPs of the other species (Figure S9).

Higher grafting densities of 0.15 and 0.2 chains/σ^2 allowed the top and bottom layers of NPs to retain hexagonal order, but interestingly did *not* lead to the close-packed, hexagonal bilayer configuration depicted in Figure S7 that maximizes the number of NP-NP contacts across the interface. Instead, the two NP layers stretched apart, shifted, and rotated relative to

DOI: 10.1021/acsnano.8b08733
ACS Nano 2019, 13, 4111−4123

each other (Figure S10a,b), while remaining stably bound to one another. These deviations, which increase in going from $\Gamma_g = 0.15$ to 0.2 chains/σ^2, obviously arise from the stronger steric repulsion that the two NP layers experience due to the NP grafts, which are now present at a higher density. The separation, shift, and rotation of the NP layers helps alleviate some of this repulsion by creating larger voids for the grafts in between the two layers and also freeing up grafts on some of the exposed NPs at the monolayer corners. Whether the two layers remain bound for $N \to \infty$ and retain the same orientation obtained here, and whether fine-tuning of the grafting density within the 0.1−0.15 chains/σ^2 range not considered here yields the ideal close-packed hexagonal bilayer remain open questions. Lastly, at even higher grafting densities of 0.3 chains/σ^2, the steric repulsion between the NPs becomes so large that they are unable to even form ordered monolayers, resulting in significantly open and irregular structures (Figure S10c).

Lastly, we explored the potential of our approach to also assemble quasi-1D structures, in addition to the small clusters and quasi-2D phases demonstrated above. One strategy for promoting the formation of linear structures is through the use of NPs grafted with chains at intermediate densities, where the steric repulsion between the grafts is small enough to allow assembly along one lateral direction, but large enough to prevent assembly along both lateral directions. Specifically, the expulsion of grafts from in between two bound NPs leads to an anisotropic distribution of graft segments around the dimer, causing a third approaching NP to feel stronger steric repulsion at the contact region of the dimer as opposed to its poles. Thus, the dimer becomes more susceptible to further assembly through its poles (longitudinal axis) rather than near the contact region (perpendicular directions).[23,24] Such multibody interactions have indeed been proposed to lead to string-like NP aggregates in bulk polymers and has the potential to lead to interesting structures at interfaces.

Figure 7 provides two examples of quasi-linear structures created *via* this strategy. The first structure, exhibiting a "serpentine" morphology (Figure 7A), was obtained from further assembly of the four tilted NP dimers with $\Gamma_g = 0.3$ chains/σ^2 reported in Figure 4D, but in a bilayer of shorter matrix chains ($L_m = 5$ beads) to promote stronger multibody effects.[24] While the mechanism for the formation of the serpentine morphology is not fully known, it likely arises from the strong steric repulsion between grafts that prevents two dimers from simultaneously forming two contacts with each other and assembling into a 2D bilayer. However, the repulsion is apparently weak enough to allow the dimers to form a single contact (though one of their NPs) resulting in a "chain" of tilted dimers connected by single bonds. The linear morphology of this chain as well as the alternating nature of these bonds going back and forth between the two layers also likely arise from steric repulsion that pushes neighboring dimers into orientations that maximize the separation distance between the two noncontacting NPs. The second structure, exhibiting a "branched" morphology (Figure 7B), was achieved through the assembly of four open trimers composed of same three species of NPs used for assembling the trimers in Figure 5C-E, *except* that the two end NPs had much smaller grafting densities ($\Gamma_g = 0.1$ chains/σ^2), causing them to adopt positions slightly above and below the interfacial plane. This effect together with strong steric repulsion between end NPs

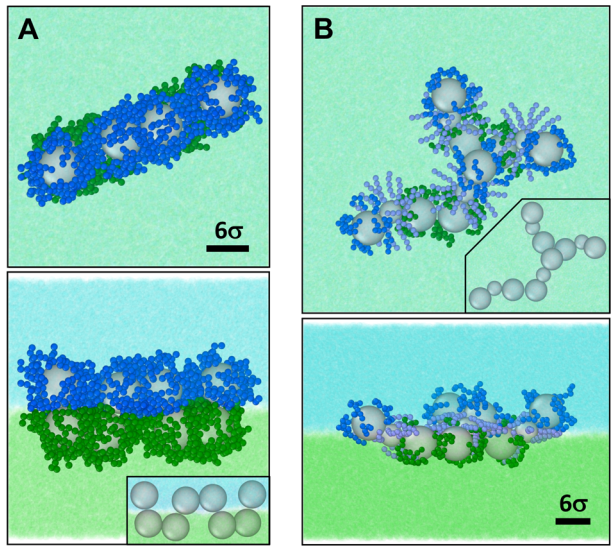

Figure 7. Quasi-linear structures of polymer-grafted NPs assembled at the interface of a bilayer: (A) Serpentine structure obtained from two antisymmetric species of NPs grafted at $\Gamma_g = 0.3$ chains/σ^2 in a bilayer of short matrix chains. (B) Branched structure obtained from the assembly of three species of NPs where the two end NPs are antisymmetric and grafted at $\Gamma_g = 0.1$ chains/σ^2. Top and bottom panels show the top and side view, and insets show structures without grafts for better visualization of NP arrangement.

that pushes them apart likely led the trimers to adopt the highly obtuse configuration observed in the figure. Interestingly, because the two end NPs of the trimer remain close to the interface, neighboring trimers could bind to each other in two ways: *via* end NPs in the same layer or *via* those on opposite layers. The former type of contact seems to permit interactions between two trimers, leading to the linear branches in the structure, while the latter apparently permits interactions between more than two trimers, leading to the branched node in the structure.

CONCLUSIONS

This study proposes and demonstrates through coarse-grained MD simulations an approach for assembling spherical NPs into anisotropic structures within a polymer matrix. The approach relies on two key ingredients—a polymer-polymer interface and polymer grafting of NPs—to break the underlying symmetry of an otherwise isotropic system of interacting particles. The polymer interface serves to introduce a finite-range, 1D harmonic field into the polymer matrix (first term in eq 1) that, *independently*, would trap NPs at the interfacial plane. The grafts, when selective to one of the polymer layers, serve to introduce a linear field (second term in eq 1), also of finite range, that displaces the harmonic trap away from the interface, the extent of which can be precisely controlled by the NP grafting density. The ability to trap multiple species of NPs differing in graft selectivity and/or graft density at distinct planes from the interface can then be used to assemble NPs into unusual and tunable structures that go beyond the isotropic, maximally close-packed assemblies nominally obtained in the bulk or at interfaces. To illustrate the potential of this approach, we demonstrated the assembly of small clusters, such as tilted dimers and open trimers with tunable orientations and bending angles, as well as quasi-1D and 2D

DOI: 10.1021/acsnano.8b08733
ACS Nano 2019, 13, 4111−4123

phases, including serpentine and branched structures, hexagonally arranged ridged monolayers, and square-packed interdigitated bilayers. We introduced a simple analytical model to provide rapid predictions of the free energies and equilibrium positions of NPs based on experimentally accessible parameters. Such a model should provide useful guidance on trapping individual NPs at desired distances from the interface. Furthermore, this model, along with one for NP-NP interaction energies, could be input into an energy-minimization algorithm to provide useful structure predictions on NP clusters and extended phases.

The ability of this approach to yield NP clusters with specific orientations or open configurations would be especially attractive for plasmonics. In this case, the NP cores could be made of a plasmonically active metal like Ag or Au, and the NP clusters could be engineered *via* polymer grafting to be stable against further assembly and exhibit nanoscopic gaps between neighboring NPs. The most obvious benefit would be the potentially unexpected plasmonic resonances that might emerge from such atypical noncontacting particle arrangements, with the additional possibility of unusual effects arising from clusters residing at the interface of two polymeric media with potentially different dielectric properties.[2,47] Furthermore, the ability of the proposed approach to tune NP configuration could enable systematic studies of structure−property relationships. Similarly assembled atypical clusters and phases of magnetic and semiconducting NPs would enable researchers to take advantage of the peculiar magnetic and exciton couplings that may emerge from such particle arrangements.[1] Other potential applications exist in the fields of solid-state catalysis, where catalytic NPs facilitating distinct reactions may be spatially organized into clusters to drive multistage reactions.[48]

The proposed approach and results presented here provide various avenues for future studies. First of all, the higher-order structures demonstrated here likely constitute only a small subset of architectures conceivable by this approach. For instance, we examined only the simplest possible scenario of two antisymmetric species of NPs to assemble quasi-2D structures, and again two or three closely related NP species to assemble quasi-1D structures. We envision that using differently sized or grafted NPs and additional species of NPs has the potential to create a vast array of exotic and interesting macroscopic phases. Similarly, it may be possible to assemble larger and more complex NP clusters (than the dimers and trimers demonstrated here) using a wider choice of polymer-grafted NP species. Second, the approach has so far been applied to spherical NPs in polymeric interfaces, but could be easily extended to other kinds of interfaces, such as those formed between oil and water, and to aspherical NPs. In the latter scenario, we envision the interfacial forces to modulate not only the position of the NPs but also their orientation. Third, the quantitative model developed here for predicting equilibrium position of NPs could be further improved by accounting for the deformation of polymer grafts and the interface, which become severe when the NPs are located near the interface in the polymer layer incompatible with the grafts. Fourth, it would be instructive to study the translational and rotational dynamics of NPs and their clusters trapped at or near interfaces, which are expected to differ substationally from their dynamics in the bulk. Another topic that demands further examination is the role of multibody effects in the interfacial assembly of higher-order structures. These effects were cursorily used in this study to demonstrate assembly of quasi-linear structures, but its full potential in particle assembly at interfaces remains to be explored. Finally, the proposed assembly approach would need to be experimentally validated. Indeed, experiments have already successfully demonstrated the ability to prepare stable polymer bilayers from mutually immiscible polymers and to preferentially capture NPs within one of the layers.[49] Future experiments on the entrapment and assembly of multiple species of NPs in such bilayers should reveal the possibilities and caveats of this interface-mediated NP assembly approach.

METHODS

Coarse-Grained Model. The grafted and matrix polymer chains, denoted by "g" and "p_1" and "p_2", were treated as Kremer−Grest bead-chains,[37] in which polymer segments, typically a few monomers long, are represented by beads of size σ and mass m. The chain lengths of both matrix polymers were fixed at $L_p = 10$ segments (beads). The length of the grafts were varied in the range $L_g = 5-20$ segments, that is, from half to twice as long as the matrix chains. The NP cores were treated as rigid spheres of radius $R_{NP} = 3\sigma$ and mass $m_{NP} = 216m$ (unless otherwise stated) with uniformly distributed grafting points across their surface. We explored grafting densities in the range $\Gamma_g = 0$ (bare NPs) to 0.4 chains/σ^2 (unless otherwise stated). Calculations based on *unperturbed* radii of gyration R_g^* of grafts (*i.e.*, in the free state *not* attached to the NPs) yielded fractional surface coverages $\Gamma_g R_g^{*2}$ of 0.1−1.85, indicating that we explored a range of grafting regimes, from mushroom to weak-brush regimes.

Adjacent beads along the chain representing bonded segments were connected to each other using a combination of a finitely extensible nonlinear elastic (FENE) spring and a Weeks−Chandler−Anderson (WCA) potential:[50]

$$U_b = U_{FENE} + U_{WCA} \tag{2}$$

where the FENE potential ensures that the bonds between segments do not stretch beyond a given separation distance of $R_0 = 1.5\sigma$ and is given by

$$U_{FENE}(r; k, R_0) = -\frac{k}{2}R_0^2 \ln\left[1 - \left(\frac{r}{R_0}\right)^2\right] \tag{3}$$

where r is the distance between the bonded segments, $k = 30\varepsilon/\sigma^2$ is the spring constant, and ε is an energy parameter. The WCA potential is a short-range purely repulsive potential given by

$$U_{WCA}(r; \sigma, \varepsilon) = \begin{cases} 4\varepsilon\left[\left(\frac{\sigma}{r}\right)^{12} - \left(\frac{\sigma}{r}\right)^{6} + \frac{1}{4}\right] & r < 2^{1/6}\sigma \\ 0 & r \geq 2^{1/6}\sigma \end{cases} \tag{4}$$

that accounts for the excluded volume interactions between the bonded segments.

The interactions between nonbonded segments, both intra- and interchain, were treated differently based on whether the parent chains were mutually miscible or immiscible, with the former exhibiting attractive interactions on top of excluded volume interactions and the latter exhibiting only excluded volume interactions, similar to approaches adopted in earlier studies.[39−41,51] Chains of the same polymer type were considered miscible, and their segmental interactions were treated using a cut-and-shifted Lennard-Jones (LJ) potential

DOI: 10.1021/acsnano.8b08733
ACS Nano 2019, 13, 4111−4123

$$U_{nb}^{\alpha\text{-}\alpha} = U_{LJ}(r;\sigma,\varepsilon,r_c) = \begin{cases} 4\varepsilon\left[\left(\frac{\sigma}{r}\right)^{12} - \left(\frac{\sigma}{r}\right)^{6} - \left(\frac{\sigma}{r_c}\right)^{12} + \left(\frac{\sigma}{r_c}\right)^{6}\right] & r < r_c \\ 0 & r \geq r_c \end{cases} \quad (5)$$

where α = g, p_1, and p_2, $r_c = 2.5\sigma$ is the cutoff distance of the potential, and ε represents the common strength of all such nonbonded interactions irrespective of chain type. Segments of the two polymer layers considered immiscible interacted with each other *via* the same WCA potential as that used for describing excluded volume interactions between bonded segments:

$$U_{nb}^{p_1\text{-}p_2} = U_{WCA}(r;\sigma,\varepsilon) \quad (6)$$

The grafts were generally considered to be compatible with one polymer layer and incompatible with the other. The former interactions were again treated using the LJ potential with an intersegmental attraction strength of ε_g and the latter using the WCA potential

$$U_{nb}^{g\text{-}\alpha} = \begin{cases} U_{LJ}(r;\sigma,\varepsilon_g,r_c) & \alpha \text{ is miscible} \\ U_{WCA}(r;\sigma,\varepsilon) & \alpha \text{ is immiscible} \end{cases} \quad (7)$$

where $\alpha = p_1$ or p_2. We explored values of ε_g between 0.5 and 2ε, that is, from half to twice as strong as the attractive interactions between polymer segments of the same kind.

The excluded volume interactions between NP cores and the polymer segments were treated using an expanded WCA potential that accounts for the larger excluded volume of the cores (compared to polymer segments):

$$U_{nb}^{NP\text{-}\alpha} = U_{WCA}(r - r_{ev};\sigma,\varepsilon) \quad (8)$$

where α = g, p_1, and p_2, r is the distance between the center of the NP core and the polymer segment, and $r_{ev} \equiv R_{NP} - \sigma/2$ is a distance shift implemented to prevent the polymer segments from penetrating the NP core. The NP cores interact with each other *via* an expanded LJ potential:

$$U_{nb}^{NP\text{-}NP} = U_{LJ}(r - 2R_{NP};\sigma,\varepsilon_{NP},r_c) \quad (9)$$

where r is the distance between the centers of the cores of NP, $2r_{NP}$ shift prevents the NP cores from penetrating each other, and a strong attraction $\varepsilon_{NP} = 50\varepsilon$ was implemented to promote NP assembly. This attraction strength is consistent with the typical van der Waals interactions between small NPs and, importantly, is also sufficiently strong to allow the NPs to overcome the steric repulsion arising from their grafts to assemble and weak enough to favor the formation of interfacial over bulk structures in the presence of an interface. More details on these three calculations are provided in the Supporting Information. The grafted chains were tethered onto the surface of the NP *via* FENE springs and with a pseudo-uniform distribution of grafting points at desired grafting density using the "generalized spiral points" algorithm of Rakhmanov *et al.*[52]

Table S1 summarizes values of all the CG model parameters considered in this study. Note that all simulation parameters and quantities are defined in units of σ, m, and ε, which set the respective length, mass, and time scales in this study.

Molecular Dynamics Simulations. All molecular dynamics (MD) simulations of the NP-polymer system were carried out using the LAMMPS package[53] developed by the Sandia National Laboratory. The simulations were carried out in the canonical (NVT) ensemble at a temperature of $T = \varepsilon/k_B$ and a polymer-segment number density of $\rho = 0.85/\sigma^3$ in the polymer bulk. Under these conditions, the chains in each polymer layer are present in a melt-like state. A velocity-Verlet algorithm with a time step of $\Delta t = 0.002(m\sigma^2/\varepsilon)^{1/2}$ was used for integrating the equations of motion, and a Nosé–Hoover thermostat with a time constant of $\tau = 1.0(m\sigma^2/\varepsilon)^{1/2}$ was used for regulating the system temperature. The polymer bilayer was confined in the z direction normal to the interface by two impermeable LJ walls, while periodic boundary conditions (PBCs) were implemented in the x and y directions parallel to the interface. The polymer layers were *each* chosen to have a thickness of $\Delta h = 15\sigma$ (or $\Delta h = 22\sigma$ for NPs with long grafts). Considering that the effective diameters of the NPs are roughly $6-12\sigma$ (depending on the length and extent of grafting), the polymer layers are sufficiently thick to capture the entire range of influence of the interface without distortion by the enclosing walls. Similarly, the simulation box was kept sufficiently large in the two lateral directions to ensure that a NP or its aggregate does not indirectly interact with itself *via* hydrodynamic flows (generated by NP mobility) propagated and reinforced through PBCs. Table S1 provides the size of simulation boxes considered in this study.

To carry out productive MD simulations for yielding meaningful data on NP dynamics, entrapment, self-assembly and free energies, we first generated well-equilibrated system of polymer-grafted NPs located at desired initial positions within a phase-separated polymer bilayer. This was achieved by first placing the required number of NPs and matrix chains in a non-overlapping configuration in a simulation box 30–50 times larger than the required dimensions. To avoid overlaps, the grafts were arranged in straight, ground-state configurations perpendicular to the NP surface, the NPs were placed sufficiently far from each other, and the two types of matrix chains were organized into loose bundles of straight chains that were respectively placed above and below the NPs. Next, we assigned Maxwell–Boltzmann-distributed velocities to all segments and performed MD simulations for 0.1–0.4 million time steps, keeping the NP locations fixed at their initial positions. This allowed the grafted and matrix chains to randomize their configurations and also spread across the simulation box to form a uniform low-density matrix. Following this, we slowly compressed the simulation box over 1 million time steps until the required dimensions consistent with the target density ρ were achieved and the two matrix polymers phase-separated into a stable bilayer. Simultaneously, the NPs were gradually moved to their desired positions within the box. Finally, the system was simulated for an additional 1 million MD time steps, holding the particles fixed at their desired locations, to further equilibrate the system.

We carried out *two* different types of simulations following equilibration. First, we carried out equilibrium simulations of *freely mobile* NPs within the bilayer for exploring the dynamics of individual NPs, especially their equilibrium positioning at or close to the interface, and for exploring the self-assembly of multiple such trapped NPs into higher-order structures. These simulations were generally started with NPs in the polymer layer most compatible with the NP grafts, specifically in the bulk region where the NPs "feel" neither the interface nor the wall, for example, $z \sim \pm 5-7\sigma$. These simulations were typically performed for 12 million time steps and the trajectories of the NPs were recorded every 100 time steps.

Second, we carried out simulations of a single *constrained* NP at different fixed distances from the interface, which were used for computing the system free energy—the potential of mean force (PMF)—as a function of the normal coordinate z of the NP. In these simulations, the NP center was held fixed at equidistant points (spaced $\Delta z = 0.5\sigma$ apart) along a normal path starting in the bulk region of one polymer layer at $z = -9\sigma$, crossing the interfacial plane at $z = 0$, and ending in the bulk of the second layer at $z = 9\sigma$ (or $z = -10\sigma$ to 10σ for NPs with longer grafts). The NP center was held fixed for 0.6 million time steps at each z location, and the ensemble-averaged normal force $\langle f_z(t)\rangle$ experienced by the NP was measured from the last 0.5 million time steps. All simulations was repeated four times to improve accuracy, yielding a total of ~100 million time steps for the entire procedure. The PMF was then computed by integrating the force component over position as

$$\Delta F(z) \equiv F(z) - F(z_0) = -\int_{z_0}^{z} f_z(z)dz \quad (10)$$

DOI: 10.1021/acsnano.8b08733
ACS Nano 2019, 13, 4111–4123

where z_0 represents a position in the bulk of the polymer layer most compatible with the NP grafts where the net force experienced by the particle is expected to be zero, that is, $f_z(z_0) \sim 0$. In the case of bare NPs, the "reference" position z_0 can be present in either layer (which are both neutral to NP core). More details of this approach for computing PMFs are provided in our earlier publication.[24]

ASSOCIATED CONTENT

Supporting Information

The Supporting Information is available free of charge on the ACS Publications website at DOI: 10.1021/acsnano.8b08733.

Choice of NP-NP attraction strength; derivation of theoretical model of NP trapping; surface tension calculations; Table of parameter values; deformations of the interface and NP grafts; comparison of tilt angles from model and simulations; comparison of equilibrium positions from model *versus* simulations; surface energy difference across two layers *versus* NP grafting density; ideal particle arrangements in square and hexagonal bilayers; hexagonal monolayer of single species of grafted NPs; and higher-order structures obtained at high grafting densities and using unequal numbers of NP species (PDF)

AUTHOR INFORMATION

Corresponding Author

*E-mail: gaurav.arya@duke.edu.

ORCID

Gaurav Arya: 0000-0002-5615-0521

Author Contributions

[§]These authors contributed equally to this work

Notes

The authors declare no competing financial interest.

ACKNOWLEDGMENTS

We thank the National Science Foundation (CMMI award 1636356) for support of this research. Computational resources were provided by the Extreme Science and Engineering Discovery Environment (XSEDE) Program supported by the National Science Foundation (ACI-1053575) and the Duke Compute Cluster (DCC). We thank Dr. Andrea Tao for useful discussions.

REFERENCES

(1) Nie, Z.; Petukhova, A.; Kumacheva, E. Properties and Emerging Applications of Self-Assembled Structures Made from Inorganic Nanoparticles. *Nat. Nanotechnol.* **2010**, *5*, 15.

(2) Hsu, S.-W.; Rodarte, A. L.; Som, M.; Arya, G.; Tao, A. R. Colloidal Plasmonic Nanocomposites: From Fabrication to Optical Function. *Chem. Rev.* **2018**, *118*, 3100−3120.

(3) Fan, J. A.; Wu, C.; Bao, K.; Bao, J.; Bardhan, R.; Halas, N. J.; Manoharan, V. N.; Nordlander, P.; Shvets, G.; Capasso, F. Self-Assembled Plasmonic Nanoparticle Clusters. *Science* **2010**, *328*, 1135−1138.

(4) Kang, Y.; Erickson, K. J.; Taton, T. A. Plasmonic Nanoparticle Chains *via* a Morphological, Sphere-to-String Transition. *J. Am. Chem. Soc.* **2005**, *127*, 13800−13801.

(5) Spinelli, P.; Hebbink, M.; De Waele, R.; Black, L.; Lenzmann, F.; Polman, A. Optical Impedance Matching using Coupled Plasmonic Nanoparticle Arrays. *Nano Lett.* **2011**, *11*, 1760−1765.

(6) Theiss, J.; Pavaskar, P.; Echternach, P. M.; Muller, R. E.; Cronin, S. B. Plasmonic Nanoparticle Arrays with Nanometer Separation for High-Performance SERS Substrates. *Nano Lett.* **2010**, *10*, 2749−2754.

(7) Nakata, K.; Hu, Y.; Uzun, O.; Bakr, O.; Stellacci, F. Chains of Superparamagnetic Nanoparticles. *Adv. Mater.* **2008**, *20*, 4294−4299.

(8) Lalatonne, Y.; Motte, L.; Russier, V.; Ngo, A.; Bonville, P.; Pileni, M. Mesoscopic Structures of Nanocrystals: Collective Magnetic Properties due to the Alignment of Nanocrystals. *J. Phys. Chem. B* **2004**, *108*, 1848−1854.

(9) Koole, R.; Liljeroth, P.; de Mello Donegá, C.; Vanmaekelbergh, D.; Meijerink, A. Electronic Coupling and Exciton Energy Transfer in CdTe Quantum-Dot Molecules. *J. Am. Chem. Soc.* **2006**, *128*, 10436−10441.

(10) Govorov, A. O.; Bryant, G. W.; Zhang, W.; Skeini, T.; Lee, J.; Kotov, N. A.; Slocik, J. M.; Naik, R. R. Exciton-Plasmon Interaction and Hybrid Excitons in Semiconductor-Metal Nanoparticle Assemblies. *Nano Lett.* **2006**, *6*, 984−994.

(11) Kulakovich, O.; Strekal, N.; Yaroshevich, A.; Maskevich, S.; Gaponenko, S.; Nabiev, I.; Woggon, U.; Artemyev, M. Enhanced Luminescence of CdSe Quantum Dots on Gold Colloids. *Nano Lett.* **2002**, *2*, 1449−1452.

(12) Balazs, A. C.; Emrick, T.; Russell, T. P. Nanoparticle Polymer Composites: Where Two Small Worlds Meet. *Science* **2006**, *314*, 1107−1110.

(13) Genix, A.-C.; Oberdisse, J. Nanoparticle Self-Assembly: From Interactions in Suspension to Polymer Nanocomposites. *Soft Matter* **2018**, *14*, 5161−5179.

(14) Murthy, C. R.; Gao, B.; Tao, A. R.; Arya, G. Automated Quantitative Image Analysis of Nanoparticle Assembly. *Nanoscale* **2015**, *7*, 9793−9805.

(15) Glotzer, S. C.; Solomon, M. J. Anisotropy of Building Blocks and their Assembly into Complex Structures. *Nat. Mater.* **2007**, *6*, 557.

(16) Chen, M.; Kim, J.; Liu, J.; Fan, H.; Sun, S. Synthesis of FePt Nanocubes and their Oriented Self-Assembly. *J. Am. Chem. Soc.* **2006**, *128*, 7132−7133.

(17) Pietrobon, B.; McEachran, M.; Kitaev, V. Synthesis of Size-Controlled Faceted Pentagonal Silver Nanorods with Tunable Plasmonic Properties and Self-Assembly of these Nanorods. *ACS Nano* **2009**, *3*, 21−26.

(18) Gao, B.; Arya, G.; Tao, A. R. Self-Orienting Nanocubes for the Assembly of Plasmonic Nanojunctions. *Nat. Nanotechnol.* **2012**, *7*, 433.

(19) Xu, X.; Rosi, N. L.; Wang, Y.; Huo, F.; Mirkin, C. A. Asymmetric Functionalization of Gold Nanoparticles with Oligonucleotides. *J. Am. Chem. Soc.* **2006**, *128*, 9286−9287.

(20) Zhang, Z.; Glotzer, S. C. Self-Assembly of Patchy Particles. *Nano Lett.* **2004**, *4*, 1407−1413.

(21) Du, J.; O'Reilly, R. K. Anisotropic Particles with Patchy, Multicompartment and Janus Architectures: Preparation and Application. *Chem. Soc. Rev.* **2011**, *40*, 2402−2416.

(22) Kumar, S. K.; Jouault, N.; Benicewicz, B.; Neely, T. Nanocomposites with Polymer Grafted Nanoparticles. *Macromolecules* **2013**, *46*, 3199−3214.

(23) Akcora, P.; Liu, H.; Kumar, S. K.; Moll, J.; Li, Y.; Benicewicz, B. C.; Schadler, L. S.; Acehan, D.; Panagiotopoulos, A. Z.; Pryamitsyn, V.; Ilavsky, J.; Thiyagarajan, P.; Colby, R. H.; Douglas, J. F. Anisotropic Self-Assembly of Spherical Polymer-Grafted Nanoparticles. *Nat. Mater.* **2009**, *8*, 354.

(24) Tang, T.-Y.; Arya, G. Anisotropic Three-Particle Interactions between Spherical Polymer-Grafted Nanoparticles in a Polymer Matrix. *Macromolecules* **2017**, *50*, 1167−1183.

(25) Kim, B. J.; Bang, J.; Hawker, C. J.; Chiu, J. J.; Pine, D. J.; Jang, S. G.; Yang, S.-M.; Kramer, E. J. Creating Surfactant Nanoparticles for Block Copolymer Composites through Surface Chemistry. *Langmuir* **2007**, *23*, 12693−12703.

(26) Lopes, W. A.; Jaeger, H. M. Hierarchical Self-Assembly of Metal Nanostructures on Diblock Copolymer Scaffolds. *Nature* **2001**, *414*, 735.

(27) Bockstaller, M. R.; Lapetnikov, Y.; Margel, S.; Thomas, E. L. Size-Selective Organization of Enthalpic Compatibilized Nanocrystals

DOI: 10.1021/acsnano.8b08733
ACS Nano 2019, 13, 4111−4123

in Ternary Block Copolymer/Particle Mixtures. *J. Am. Chem. Soc.* **2003**, *125*, 5276−5277.
(28) Sohn, B.-H.; Choi, J.-M.; Yoo, S. I.; Yun, S.-H.; Zin, W.-C.; Jung, J. C.; Kanehara, M.; Hirata, T.; Teranishi, T. Directed Self-Assembly of Two Kinds of Nanoparticles Utilizing Monolayer Films of Diblock Copolymer Micelles. *J. Am. Chem. Soc.* **2003**, *125*, 6368−6369.
(29) Zhang, Q.; Xu, T.; Butterfield, D.; Misner, M. J.; Ryu, D. Y.; Emrick, T.; Russell, T. P. Controlled Placement of CdSe Nanoparticles in Diblock Copolymer Templates by Electrophoretic Deposition. *Nano Lett.* **2005**, *5*, 357−361.
(30) Erb, R. M.; Son, H. S.; Samanta, B.; Rotello, V. M.; Yellen, B. B. Magnetic Assembly of Colloidal Superstructures with Multipole Symmetry. *Nature* **2009**, *457*, 999.
(31) Gangwal, S.; Cayre, O. J.; Velev, O. D. Dielectrophoretic Assembly of Metallodielectric Janus Particles in AC Electric Fields. *Langmuir* **2008**, *24*, 13312−13320.
(32) Singh, J. P.; Lele, P. P.; Nettesheim, F.; Wagner, N. J.; Furst, E. M. One-and Two-Dimensional Assembly of Colloidal Ellipsoids in AC Electric Fields. *Phys. Rev. E* **2009**, *79*, 050401.
(33) Pieranski, P. Two-Dimensional Interfacial Colloidal Crystals. *Phys. Rev. Lett.* **1980**, *45*, 569.
(34) Binks, B. P.; Horozov, T. S. *Colloidal Particles at Liquid Interfaces*; Cambridge University Press: Cambridge, 2006.
(35) Böker, A.; He, J.; Emrick, T.; Russell, T. P. Self-Assembly of Nanoparticles at Interfaces. *Soft Matter* **2007**, *3*, 1231−1248.
(36) Bresme, F.; Oettel, M. Nanoparticles at Fluid Interfaces. *J. Phys.: Condens. Matter* **2007**, *19*, 413101.
(37) Kremer, K.; Grest, G. S. Dynamics of Entangled Linear Polymer Melts: A Molecular-Dynamics Simulation. *J. Chem. Phys.* **1990**, *92*, 5057−5086.
(38) Hattemer, G. D.; Arya, G. Viscoelastic Properties of Polymer-Grafted Nanoparticle Composites from Molecular Dynamics Simulations. *Macromolecules* **2015**, *48*, 1240−1255.
(39) Cheung, D. L. Molecular Dynamics Study of Nanoparticle Stability at Liquid Interfaces: Effect of Nanoparticle-Solvent Interaction and Capillary Waves. *J. Chem. Phys.* **2011**, *135*, 054704.
(40) Galliero, G. Lennard-Jones Fluid-Fluid Interfaces Under Shear. *Phys. Rev. E* **2010**, *81*, 056306.
(41) Rezvantalab, H.; Shojaei-Zadeh, S. Tilting and Tumbling of Janus Nanoparticles at Sheared Interfaces. *ACS Nano* **2016**, *10*, 5354−5361.
(42) Levine, S.; Bowen, B. D.; Partridge, S. J. Stabilization of Emulsions by Fine Particles I. Partitioning of Particles between Continuous Phase and Oil/Water Interface. *Colloids Surf.* **1989**, *38*, 325−343.
(43) Lin, Y.; Skaff, H.; Emrick, T.; Dinsmore, A.; Russell, T. P. Nanoparticle Assembly and Transport at Liquid-Liquid Interfaces. *Science* **2003**, *299*, 226−229.
(44) Arkus, N.; Manoharan, V. N.; Brenner, M. P. Minimal Energy Clusters of Hard Spheres with Short Range Attractions. *Phys. Rev. Lett.* **2009**, *103*, 118303.
(45) Mossa, S.; Sciortino, F.; Tartaglia, P.; Zaccarelli, E. Ground-State Clusters for Short-Range Attractive and Long-Range Repulsive Potentials. *Langmuir* **2004**, *20*, 10756−10763.
(46) Xie, Q.; Davies, G. B.; Harting, J. Direct Assembly of Magnetic Janus Particles at a Droplet Interface. *ACS Nano* **2017**, *11*, 11232−11239.
(47) Sherry, L. J.; Chang, S.-H.; Schatz, G. C.; Van Duyne, R. P.; Wiley, B. J.; Xia, Y. Localized Surface Plasmon Resonance Spectroscopy of Single Silver Nanocubes. *Nano Lett.* **2005**, *5*, 2034−2038.
(48) Ferrando, R.; Jellinek, J.; Johnston, R. L. Nanoalloys: From Theory to Applications of Alloy Clusters and Nanoparticles. *Chem. Rev.* **2008**, *108*, 845−910.
(49) Hsu, S.-W.; Long, Y.; Subramanian, A. G.; Tao, A. R. Directed Assembly of Metal Nanoparticles in Polymer Bilayers. *Mol. Sys. Des. Eng.* **2018**, *3*, 390−396.
(50) Weeks, J. D.; Chandler, D.; Andersen, H. C. Role of Repulsive Forces in Determining the Equilibrium Structure of Simple Liquids. *J. Chem. Phys.* **1971**, *54*, 5237−5247.
(51) Padilla, P.; Toxvaerd, S.; Stecki, J. Shear Flow at Liquid−Liquid Interfaces. *J. Chem. Phys.* **1995**, *103*, 716−724.
(52) Rakhmanov, E. A.; Saff, E.; Zhou, Y. Minimal Discrete Energy on the Sphere. *Math. Res. Lett.* **1994**, *1*, 647−662.
(53) Plimpton, S. Fast Parallel Algorithms for Short-Range Molecular Dynamics. *J. Comput. Phys.* **1995**, *117*, 1−19.

DOI: 10.1021/acsnano.8b08733
ACS Nano 2019, 13, 4111−4123